Tellus SERIES B CHEMICAL AND PHYSICAL METEOROLOGY
PUBLISHED BY THE INTERNATIONAL METEOROLOGICAL INSTITUTE IN STOCKHOLM

Tellus (2010), 62B, 228–241
Printed in Singapore. All rights reserved

TELLUS

Year round measurements of O_3 and CO at a rural site near Beijing: variations in their correlations

By YUXUAN WANG[1]*, JIMING HAO[1], MICHAEL B. MCELROY[2], J. WILLIAM MUNGER[2], HONG MA[1], CHRIS P. NIELSEN[3] and YUQIANG ZHANG[1], [1]*Department of Environmental Science and Engineering and State Key Joint Laboratory of Environment Simulation and Pollution, Tsinghua University, Beijing 100084, China*; [2]*Department of Earth and Planetary Sciences and School of Engineering and Applied Sciences, Harvard University, Cambridge, MA, USA*; [3]*Harvard China Project and School of Engineering and Applied Sciences, Harvard University, Cambridge, MA, USA*

(Manuscript received 19 October 2009; in final form 21 May 2010)

ABSTRACT

We examine seasonal variations of carbon monoxide (CO), ozone (O_3), and their relationships observed over the course of 3 yr (2005–2007) at Miyun, a rural site 100 km north of Beijing. Monthly mean afternoon mixing ratios of CO have broad maxima in winter and a secondary peak in June. Monthly mean afternoon O_3 shows a clear seasonal pattern with a major peak in June (85 ppb), a secondary peak in September (65 ppb) and minimum in winter (50–55 ppb). The seasonal cycles of O_3 and CO are associated with seasonal changes in dominant synoptic pattern. Substantial interannual variability is found for CO which is attributed to the interannual variability of meteorology and emissions from biomass burning. The seasonality and magnitude of background CO and O_3 derived at Miyun are consistent with observations at upwind remote continental sites. The O_3–CO correlation slope is about 0.07 ppb ppb^{-1} on average in summer, significantly lower than the typical slope of 0.3 ppb ppb^{-1} reported for developed countries. The O_3–CO correlation slope shows large gradients for different types of air masses (0.133 $\pm$ 0.017 ppb ppb^{-1} in aged urban pollution plumes and 0.047 $\pm$ 0.008 ppb ppb^{-1} in biomass burning plumes), suggesting that the conventional method of direct scaling the mean O_3–CO slope by CO emissions to deduce O_3 production rate is subject to large uncertainties if applied for China.

1. Introduction

Ozone (O_3) is a critical atmospheric species responsible for the oxidizing power of the troposphere. It is produced in the troposphere by chemical processes triggered by emissions of volatile organic compounds (VOCs) and carbon monoxide (CO) in the presence of NO_x. It is also transported from the stratosphere. CO is a relatively long-lived tracer of a variety of combustion sources (especially transportation and biomass burning), with additional sources from in situ oxidation of hydrocarbons in summer. Reaction with OH is the dominant sink for CO in the atmosphere contributing to a relative long lifetime (2–5 months).

The correlation of O_3 and CO has been used in many studies to examine the influences of anthropogenic precursors on O_3 (Poulida et al., 1991; Chin et al., 1994; Parrish et al., 1998; Mao and Talbot, 2004) and has provided a good indication of long-range transport of O_3 (Zhang et al., 2008). The O_3–CO relationship was shown to be a more robust chemical signature of cyclone airstreams than mixing ratios of individual species (Cooper et al., 2002). A positive correlation, observed typically in summer, would indicate photochemical production of O_3 resulting from anthropogenic sources, while a negative correlation would suggest removal of O_3 by anthropogenic emissions or the influences of stratospheric air masses. Other factors such as loss of O_3 by deposition at the surface and vertical mixing also influence the O_3–CO correlations. The O_3–CO correlations are used to deduce photochemical production rates and export fluxes of anthropogenic O_3 out of a major source region (Parrish et al., 1993; Mauzerall et al., 2000), but such direct interpretation is subject to uncertainties due to confounding factors such as the large-scale gradients along the plume, O_3 deposition during transit, and chemical sources/sinks of CO (Chin et al., 1994; Pfister et al., 2006; Real et al., 2008).

The relationships between O_3 and CO have been observed at many surface sites in developed regions (e.g. North America, Western Europe and Japan), where the O_3–CO correlation slope ranges from 0.2 to 0.4 ppb ppb^{-1} in summer with a typical value of 0.3 ppb ppb^{-1} (Chin et al., 1994; Parrish et al., 1998;

*Corresponding author.
e-mail: yxw@tsinghua.edu.cn
DOI: 10.1111/j.1600-0889.2010.00464.x

Mauzerall et al., 2000; Pochanart et al., 2003; Mao and Talbot, 2004). Such observations have been sparse, however, over large developing countries such as China where anthropogenic emissions of O_3 precursors have been rapidly rising with significant implications for the global atmosphere (Ohara et al., 2007; Zhang et al., 2007). Previous surface measurements in China suggested strong positive correlations of O_3 and CO in east China in summertime (Wang et al., 2001; Gao et al., 2005), but only weak correlations in springtime (Wang et al., 2003, 2004). This seasonal pattern is similar to what is observed in North America (Poulida et al., 1991; Parrish et al., 1998; Mao and Talbot, 2004). Wang et al. (2006b) found negative correlations of O_3 and CO in summertime at a remote mountain site (Mt. Waliguan) on the Tibetan Plateau in west China, suggesting a stratospheric origin for ozone observed at this site in summer. The O_3–CO ratios measured in China were found to be much smaller (<0.1 ppb ppb^{-1}) than those in North America (0.3–0.4 ppb ppb^{-1}), presumably due to a larger emission ratio of CO relative to NO_x in China. The implication of low O_3–CO correlation ratios in China on photochemical production and loss of ozone for the region has not been well studied.

This study examines continuous measurements of surface O_3 and CO over the course of 3 yr (2005–2007) at Miyun, a rural site 100 km northeast of Beijing urban centre. The location of the site provides an opportunity to sample both the Beijing pollution outflow and the relative clean continental background air masses flowing in from the north. The relative frequency of the two types of air masses observed at the site shows a seasonal pattern as a result of the monsoonal meteorology. Considering the large-scale, regional influences of the monsoon, the seasonal variability of CO and O_3 observed at the site is expected to be representative for North China (north of Yangtze River) in general. A better understanding of factors controlling the temporal variability of O_3 and CO and their relationship at the site should shed light on regional features of transport and photochemistry. We begin in Section 2 with summaries of the observations of CO, O_3 and their relationship at Miyun. Further analyses of the data are presented in Section 3, including interannual variations, diurnal patterns, background concentrations and the gradient of O_3–CO correlation in different plumes. Summary remarks are given in Section 4.

2. Site description and summary of observations

The Miyun site (40°29′N, 116°46.45′E) is located about 100 km northeast of the Beijing urban centre. The region surrounding the site is characterized by a mix of agriculture and small villages. Due to the annual shift in monsoon pattern, cold dry winds from the northwest are more frequent in winter and warm moist southwesterly winds are more frequent in summer. The location was selected to capture the dichotomy between clean continental air and the Beijing urban plume. The measurements began in November 2004 and include continuous observations of O_3, CO, CO_2 and basic meteorological data (temperature, relative humidity, wind speed and direction). Additional instruments to measure NO, NO_y and SO_2 were added in 2006. This study focuses on measurements of O_3 and CO for a period of 3 yr (2005–2007). Details of the site and the O_3 and CO instruments are described by Wang et al. (2008).

2.1. Diurnal cycle of O_3 and CO

The daily cycle of O_3 at the surface typically exhibits maxima in the afternoon with minima at night. The amplitude of the diurnal variation reflects both the strength of photochemical production of ozone and the net balance between surface deposition and transport from aloft. Nighttime minima in vertical mixing and depth of the boundary layer allow depletion of ozone at the surface. At many rural sites, the diurnal cycle is affected by transport of O_3 and its precursors from nearby urban regions (Logan, 1989). We first examine the seasonal changes in the diurnal cycle of O_3 and CO at Miyun.

Figure 1 presents seasonal-mean diurnal variations of O_3 (a) and CO (b) measured at Miyun in winter and summer. The amplitude of the diurnal variation of O_3 averaged about 60 ppb in summer compared to only 15 ppb in winter, reflecting more active summertime photochemical production of O_3. The afternoon peak of O_3 in winter is likely due to entrainment of elevated O_3

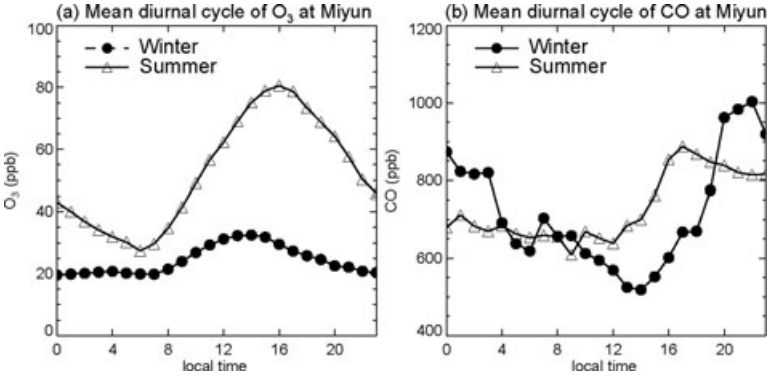

Fig. 1. Average diurnal cycles of O_3 (a) and CO (b) at Miyun in winter (dots) and summer (triangles).

from the residual layer rather than fresh photochemical production (Kleinman et al., 1994; Munger et al., 1996). The afternoon maxima of O_3 in winter coincide with the minima of CO, which is consistent with entrainment because the mixing ratio of CO tends to decrease with height.

The peak mixing ratio of O_3 in summer is shifted 2 h later to 4 p.m. as compared to 2 p.m. in winter (Fig. 1). Peak levels of O_3 coincide with peak CO in summer demonstrating the association of high O_3 production with precursors, whereas in winter the highest levels of precursors are associated with low O_3 (Fig. 1). This suggests that the shift of O_3 peak hour to later afternoon from winter to summer is due to the stronger influence of recent photochemical production in the urban plume during transport to the site in summer compared with winter.

As the boundary layer is expected to get much shallower at night, nighttime observations may be sensitive to local emissions and may not be representative of regional conditions. Observations in the afternoon when the boundary layer and strength of vertical mixing reach the maximum of the day should be more representative of regional conditions. For seasonal variations of O_3 and CO presented below, we focus on observations in the afternoon (1200–1800, local time), the typical period of daily minimum CO (see Fig. 1), from 2005 to 2007.

2.2. *Seasonal cycle of CO*

Figure 2a summarizes the month-to-month variation of afternoon CO observed at Miyun. The mean mixing ratio of CO for each month is higher than the median, and the difference can be up to a factor of two in winter and spring (November–March). Examining the distribution of CO and wind directions, we identified two distinct groups of air masses sampled at Miyun: one featuring low levels of CO (<200 ppb) reflecting relatively clean continental air masses from the north, and the other consisting of high levels of CO (>800 ppb) representing polluted air masses from the urban area in the south. This feature is illustrated in Fig. 3 showing the frequency distribution of afternoon CO mixing ratios observed in 2006 as an example. The distribution features a pronounced peak at about 160 ppb, a much smaller peak at 800 ppb and a long tail towards very high CO up to a few ppm. The difference in CO between the two air mass groups is largest in winter when emissions of CO are highest in north

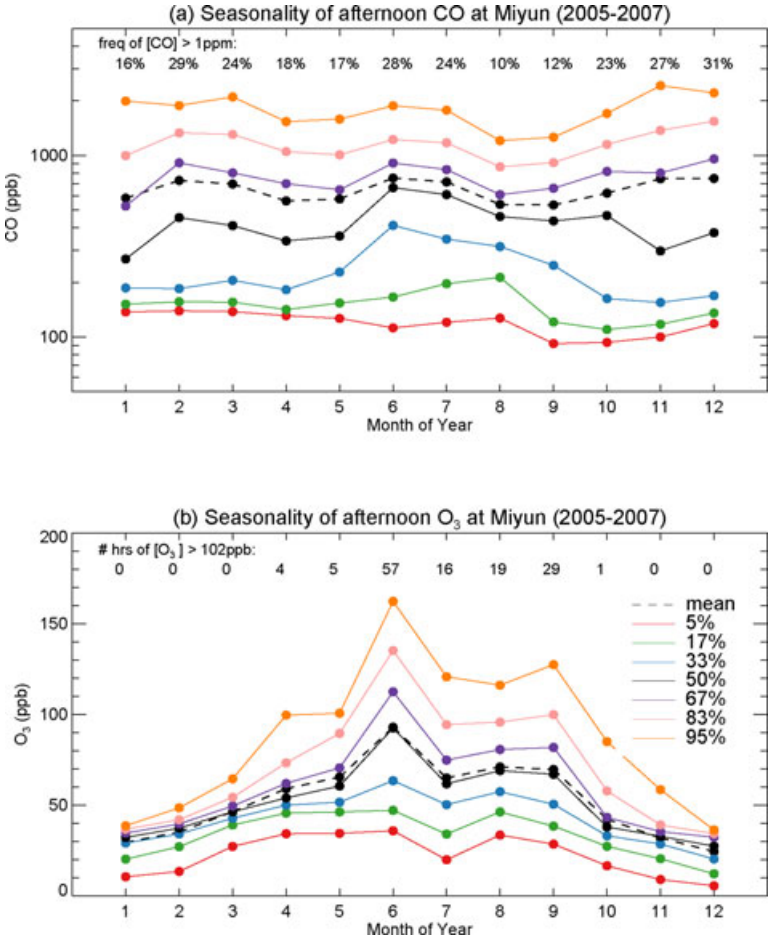

Fig. 2. Monthly variations of afternoon (1200–1800, local time) CO on a log scale (a) and O_3 on a linear scale (b) at Miyun averaged over the course of 3 yr (2005–2007). Mixing ratios at different cumulative probability percentiles are shown in coloured solid lines, and monthly mean in dashed line.

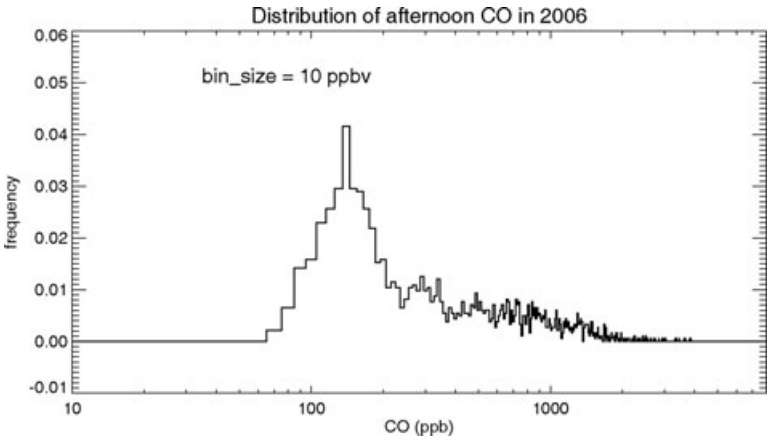

Fig. 3. Frequency distribution of afternoon CO mixing ratios observed at Miyun in 2006. The *X*-axis is on log scale.

China due to increased emissions associated with seasonal heating (Streets et al., 2006). The contrast in CO between the two types of air masses indicates that the Miyun site is well sited to sample both the relatively clean background air and the polluted regional air in China.

Because of the seasonal change in dominant synoptic pattern, the relatively clean continental air masses are sampled more frequently in winter and the polluted air masses more commonly in summer. This is shown in the different frequency distribution of afternoon CO between winter and summer (Fig. 4). The distribution in winter shows a much more pronounced peak at [CO] lower than 200 ppbv than in summer. This accounts for the seasonal cycles observed for both the lower percentiles and the median of CO at Miyun, the latter showing summer maxima at 500–600 ppb with winter minima at 300–400 ppb. The mean and upper percentiles (>67%) of CO reflect the relative frequency of urban pollution plumes sampled at the site and consequently have different seasonality compared with the median and lower percentiles. The mean and upper percentiles of CO have two peaks, one from late fall to winter (November, December, January and February) and the other in early summer (June–July), with minima during the transition season (April–May and August–September). At Miyun the annual mean afternoon mixing ratio of CO is 647 ppb, higher than observed at Lin An in the Yangtze River Delta (Wang et al., 2002) by about 60 ppb. By comparison, annual mean CO mixing ratios at rural low-elevation sites in the eastern North America are generally less than 200 ppb (Chin et al., 1994; Liang et al., 1998; Mao and Talbot, 2004). Compared with the clear seasonal pattern of maxima in winter and minima in summer reported for CO at other Chinese surface sites (Wang et al., 2002, 2005) and at mid-latitude surface sites in North America (Chin et al., 1994; Parrish et al., 1998; Mao and Talbot, 2004), the seasonal cycles of the mean and median for CO at Miyun are more complex with broad maxima in winter and secondary peaks in early summer. As discussed above, the early summer peak arises because the Miyun site is located downwind of major source regions in summer under the more frequent southerly flows.

2.3. *Seasonal cycle of ozone*

Figure 2b summarizes the month-to-month variations of afternoon O_3 observed at Miyun. The seasonal cycles of the mean and median for O_3 are similar in shape. Monthly mean afternoon

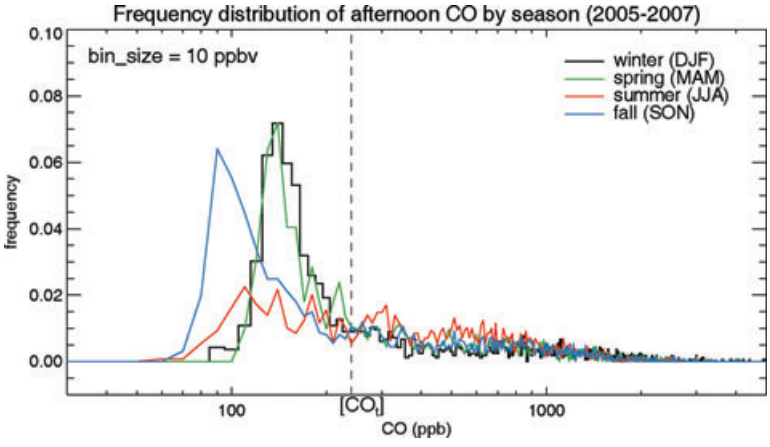

Fig. 4. Frequency distribution of afternoon CO observed at Miyun by seasons (2005–2007). The *X*-axis is on log scale.

O_3 is below 45 ppb from late fall through early spring (October–March). It increases to 50–55 ppb in April and May, reaching maxima of about 85 ppb in June, remaining relatively flat at 65 ppb from July to September. At the higher percentiles (>67%), O_3 shows a minor peak in September in addition to the major peak in June. The rapid decrease in O_3 from June to July is attributed to seasonal increases in monsoonal rainfall and cloudiness in July as optically thick clouds suppress photochemical production of O_3 (Wang et al., 2008). The seasonal cycle of O_3 at Miyun is similar to that reported for a rural site further north of Beijing (Shangdianzi) (Lin et al. 2008) and to the surface ozone climatology over Beijing derived from the MOZAIC aircraft data (Ding et al., 2008). In contrast, surface O_3 at the Lin An site in central-east China featured a maximum in May (Wang et al., 2002). The mean mixing ratio of O_3 for the peak month is 46.5 ppb (June) at Shangdianzi (55 km northeast of Miyun), 60 ppb (June) from the MOZAIC surface ozone climatology for Beijing and 56 ppb (May) from Lin An, all lower than the value of 85 ppb observed at Miyun. The secondary peak of O_3 in September at Miyun is consistent with an O_3 maximum in autumn suggested by Luo et al. (2000) based on observations in 1995 at two surface sites in North China (Qingdao and Longfeng Mountain), but their observations did not show any peaks of O_3 in summer.

The fraction of afternoon hours when 1-h averages of O_3 exceed 102 ppb (the Chinese air quality standards, 1-h concentration of 200 μg m^{-3} at 1 atm and 25 °C, corresponding to 102 ppbv) at Miyun is indicated in Fig. 2b for each month. High O_3 events occurred most frequently in June and September, with average non-attainment hours of 57 and 29, respectively, during 2005–2007. The highest hourly concentration was 197 ppb, recorded in June 2007. O_3 pollution events are also obvious in July and August. In July, for example, despite the relatively low monthly mean afternoon O_3, there were 32 non-attainment hours in July 2007, with the highest mixing ratio equal to 180 ppb.

2.4. Seasonal change in O_3–CO correlations

Figure 5 summarizes month-to-month variations in the relationships between O_3 and CO observed in afternoons (1200–1800) at Miyun. The correlation slopes were derived from the reduced-major-axis regression (Hirsch and Gilroy, 1984). As shown in Fig. 5, O_3 and CO have moderate to strong negative correlations in winter, and moderate to strong positive correlations in summer and early fall (June–September, except in July). The correlations of O_3 and CO are weak and not statistically significant in spring (March–April–May), fall (October–November) and in July. The strong negative correlations in winter imply removal of O_3 in air masses laden with high concentrations of CO originating from the Beijing urban area. CO itself does not affect O_3, but is a tracer for NO, which we presume is responsible for O_3 destruction ($NO + O_3 \rightarrow NO_2 + O_2$) that is emitted along with

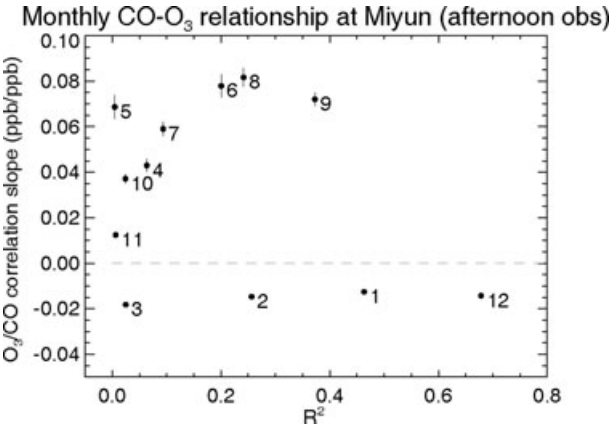

Fig. 5. Average month to month variations of the O_3–CO relationship observed in the afternoon (1200–1800, local time) at Miyun. The *X*-axis is the square of the correlation coefficients (R^2) and *Y*-axis the slope of O_3–CO correlations (ppb ppb^{-1}). The results are averages over the 3 yr (2005–2007). The slope is derived by the reduced-major-axis method. The numbers next to the dots indicate the months. The vertical line indicates the uncertainty of the correlation slope for each month.

CO (Chin et al., 1994). At low sun angles in winter, photolysis of NO_2 is too slow to regenerate significant O_3 during transport to the site. The positive correlation during the photochemically active period from June to September may be attributed to rapid photochemical production of O_3 from anthropogenic precursors during transport. The lack of a strong O_3–CO correlation in July reflects suppression of photochemical ozone production by optically thick monsoonal clouds which does not affect CO (Wang et al., 2008). The O_3–CO ratio at Miyun in summer is about 0.07 ppb ppb^{-1} on average, consistent with values inferred from observations at other Chinese sites (<0.1 ppb ppb^{-1}) (Wang et al., 2001; Gao et al., 2005), but significantly lower than values reported for surface sites in North America (0.3–0.4 ppb ppb^{-1}) (Chin et al., 1994; Parrish et al., 1998; Mao and Talbot, 2004).

As suggested by other studies (Parrish et al., 1998; Mao and Talbot, 2004), the transition between chemical removal and photochemical production of O_3 would lead to the apparent disappearance of the O_3–CO correlation. This transition period was found to occur in spring and in October–November at Miyun. For example, O_3 was positively correlated with CO in the first half of October, whereas the correlation became negative in the latter half of the month. It has been suggested also that the influence of air masses from the upper troposphere and lower stratospheric could confound O_3–CO correlations in spring for high-elevation sites (Parrish et al., 1998), but the stratospheric influence is expected to be negligible at low-elevation surface sites. We do not observe high O_3, low CO points at Miyun that are indicative of stratospheric air.

3. Discussion

3.1. Interannual variability of CO and O_3

Interannual monthly variations of afternoon CO and O_3 observed at Miyun are presented in Figs. 6a and b respectively. Significant interannual variability is observed for CO for all months. Mean CO levels are between 900 and 1000 ppb in February, March and June 2007, much higher than values of less than 700 ppb in 2005 and 2006. Measurements in June 2005 were not available due to instrumental problems. Monthly mean afternoon CO was 40% higher during October 2006 as compared to either 2005 or 2007. Despite the interannual variability of monthly mean CO, the seasonal cycle of CO is similar for individual years. Compared with CO, the interannual variability of afternoon O_3 is much smaller and not significant from late fall through early spring (November–March). Monthly mean mixing ratios for afternoon O_3 were 20–30 ppb higher during June and July 2007 as compared to 2006, consistent with the elevated CO levels during the same months in 2007.

The interannual variability of CO and O_3 can be attributed to the interannual variability of meteorology and variations in emissions such as biomass burning. Here we take June as an example. Mean afternoon CO and O_3 levels in June 2007 were 400 and 30 ppb higher than those in June 2006, respectively. The cumulative frequency distribution of afternoon CO for June of 2006 and 2007 is compared in Fig. 7a. CO levels were significantly higher in June 2007 not only at the high end of the distribution but also at the lower end. Over 80% of the data in June 2007 had CO levels exceeding 500 ppb, compared with less than 30% in June 2006. The difference in CO at the low end of the distribution (lower than the 50th percentile), representing the background and relatively clean continental air masses from the north, suggests that this type of air mass was sampled less frequently at the site in June 2007. This is consistent with measurements of local wind directions. Northerly winds were observed about 30% of the time in June 2006, decreasing to only 5% of the time in June 2007. SSW and SW winds accounted for 65% of the observations in June 2007. Although wind direction measured locally at the site is not equal to the direction from which air masses originate, there is an overall pattern driven by mountain range to the north of site that local winds with southerly component come from the plain surrounding Beijing and local winds from the north come through the mountains. The large difference

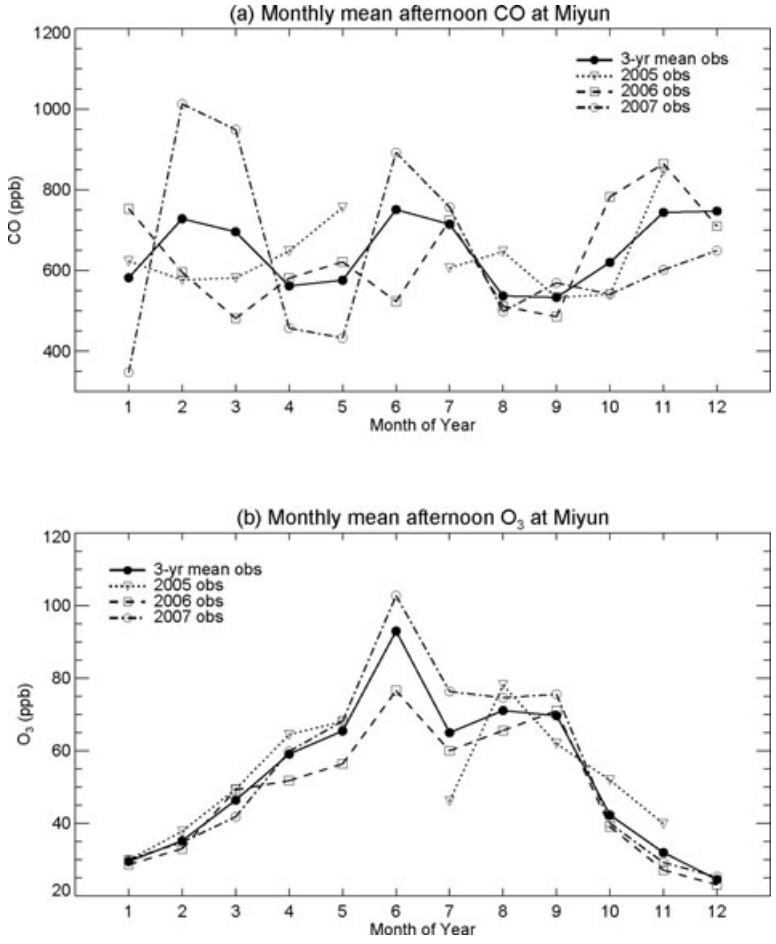

Fig. 6. Monthly mean afternoon CO (a) and O_3 (b) observed at Miyun in different years (2005–2007). The average over the 3 yr (2005–2007) is shown in solid black line.

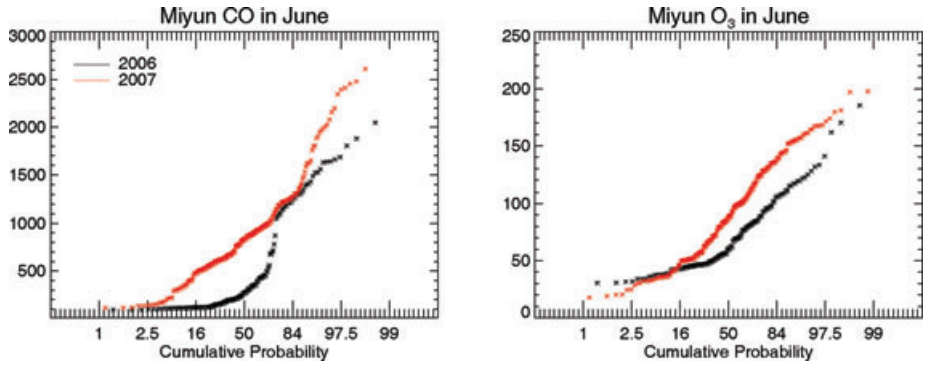

Fig. 7. Cumulative probability distribution of afternoon CO (a) and O_3 (b) observed in June 2006 (black dots) and June 2007 (red dots). Each data point represent 1-h average mixing ratio.

in the relative frequency between northerly and southwesterly winds between June 2006 and 2007 suggests a shift in synoptic weather pattern. Concentrations of CO at the high end of the distribution (above the 84th percentile), representing pollution episodes, are greater by 20% in June 2007. This suggests that polluted air masses, presumably sampling from the Beijing urban area, had significantly higher CO in June 2007 than in June 2006. Although we do not have in situ measurements in urban Beijing to compare the pollution levels between the 2 months, the monthly air quality summary provided by the Beijing Environmental Protection Bureau (EPB) reported poor air quality in June 2007 attributing this to a combination of meteorological conditions unfavourable for pollution dispersion and increases in emissions from biomass burning in regions surrounding the city (Beijing Environmental Protection Bureau, Monthly Air Quality Report (July 2007), http://www.bjepb.gov.cn/bjhb/publish/portal0/tab377/info9519.htm, read June 20, 2009).

Biomass burning is a major source of CO on both regional and global scales with large interannual variations (van der Werf et al., 2006). Biomass burning in China mainly involves crop residues (Streets et al., 2006; Fu et al., 2007). It peaks in June over North China following the harvest of winter wheat (Fu et al., 2007; Ding et al., 2008). Figure 8 displays fire spots over North China for June 2006 (a) and 2007 (b) observed by Advanced Along-Track Scanning Radiometer (ATSR). There were a total of 430 fire spots over the domain in June 2007, 70% more than the 258 fire spots identified in June 2006. Compared with June 2006, far more fire spots occurred southwest of the site in June 2007. The prevailing SW winds in this month allowed for effective transport of biomass burning emissions to the site and for their mixture with urban pollution.

Figure 7b compares the cumulative frequency distribution of afternoon O_3 between June 2006 and 2007. O_3 levels were 20–40% higher in June 2007 compared with June 2006 above the 15th percentile, consistent with the differences in CO. The difference between the years for O_3 is relatively less above the 97.5th percentile than for CO. Open burning of crop residues is known to emit much more CO than NO_x (an ozone precursor) per unit mass of fuel burned because of burning conditions (low temperature, inefficient combustion) (Wang et al., 2007), contributing thus to a lesser extent to the enhancement of O_3.

3.2. *Background CO and O_3*

Background observations of CO and O_3 provide essential input to efforts to determine the enhancement of both species resulting from anthropogenic emissions. Measurements at remote surface sites provide valuable information on this background. Based on representative measurements over North America, Europe and Japan, it is suggested that background O_3 in the northern hemisphere has increased over the past decades (Oltmans et al., 1998; Lin et al., 2000; Jaffe and Ray, 2007). This increase can

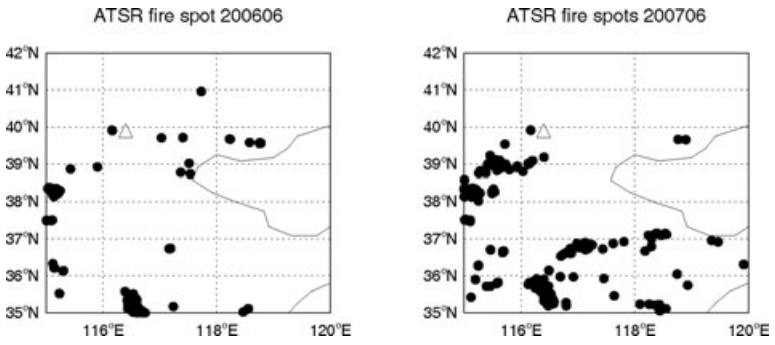

Fig. 8. Locations of fire spots obtained from ATSR over North China Plain for June 2006 (left-hand panel) and June 2007 (right-hand panel). The Miyun site is indicated as triangle.

be attributed to anthropogenic emissions of ozone precursors worldwide. Few remote sites have been established in China to provide scientific measurements of the background levels of important trace species in the atmosphere. These data are important considering the rapid increases in Chinese anthropogenic emissions.

As background defines the mixing ratio of a species that would exist without the influence of domestic anthropogenic sources, it can be derived from measurements at a surface site that can capture the characteristics of air flowing into a region. The frequency distribution of afternoon CO mixing ratios observed at Miyun is summarized in Fig. 4 by seasons (2005–2007). Because the Miyun site is located on the edge of major source regions and there is a strong gradient in emission sources between the Beijing plain and the interior mountainous regions north of Miyun (Streets et al., 2006, Wang et al., 2008), we expect that background air masses sampled at Miyun will have distinctly lower levels of primary pollutants, represented by CO in this study, than polluted regional/local air masses. As shown in Fig. 4, the presence of a narrow and pronounced peak at the lower end of the frequency distribution in winter (December, January and Feburary), spring (March, April and May) and fall (September, October and November) suggests that background air masses are frequently sampled at the site in these seasons and it is possible to extract background air masses based on the frequency distribution of CO. The lack of such a peak in summer (June, July and August) suggests that summertime measurements at this site may not be suitable for identifying the background since the site is located downwind of the Beijing urban area in summer under the prevailing southwesterly winds and is consequently poorly located to sample the relatively clean continental air masses frequently enough. We will not discuss summertime background in the following discussion, although summertime data will be presented in the figures.

The frequency distribution of CO peaks at a level lower than 150 ppbv and falls off quickly to nearly zero between 200 and 300 ppbv (Fig. 4). To extract background air masses, the distribution is truncated at a threshold level of CO (denoted as $[CO_t]$) at which the frequency distribution decreases to 0.01 after reaching the peak, as illustrated schematically in Fig. 4. $[CO_t]$ is 230, 220, 190 ppbv in winter, spring and fall, respectively. We assume that air masses contained in this portion of the distribution (i.e. observations with CO mixing ratios lower than $[CO_t]$) can be regarded as representative of the background. Background air masses account for 43, 33 and 35% of all afternoon observations in winter, spring and fall, respectively.

As shown in Fig. 4, background CO follows a lognormal distribution in non-summer seasons. The distribution is similar in winter and spring with a peak at 150 ppbv. The peak shifts to 90 ppbv in fall with a broad shoulder around 150 ppbv. The frequency distribution of O_3 in background air masses is presented in Fig. 9. The distribution of background O_3 is close to normal in non-summer seasons. It peaks between 30 and 40 ppbv in winter and fall and 45–50 ppbv in spring.

$[CO_t]$ is a key parameter in estimating background CO and O_3 at the site. In a sensitivity test in which $[CO_t]$ is set of 250 ppbv in each season, the fraction of background air masses in all afternoon observations increases by less than 10%, reaching 45, 40 and 39% in winter, spring and fall, respectively. No significant difference was found in the distribution of background O_3 as a result of this test (Fig. 9). This suggests that the distribution of background CO and O_3 is not significantly affected by $[CO_t]$. However, as $[CO_t]$ determines the tail length of the distribution, mean mixing ratios of background CO and O_3 are expected to be more sensitive.

Mean mixing ratios of background CO and O_3 at Miyun for each month are summarized in Figs. 10a and b, respectively. Background CO at Miyun ranges from 130 to 170 ppb, with a maximum in winter (December and January) and minimum in autumn (September and October). Background CO at Miyun is compared in Fig. 10a with monthly mean CO measured at two adjacent remote continental sites: Ulaan Uul (UUM) in Mongolia (44.45°N, 111.10°E, 914 m a.s.l.) included in the NOAA/ESRL (Earth System Research Laboratory) network (GLOBALVIEW-CO, 2009), and Mondy (51°39'N, 100°55'E, 2006 m a.s.l.) in East Siberia (Pochanart et al. 2003). Both UUM

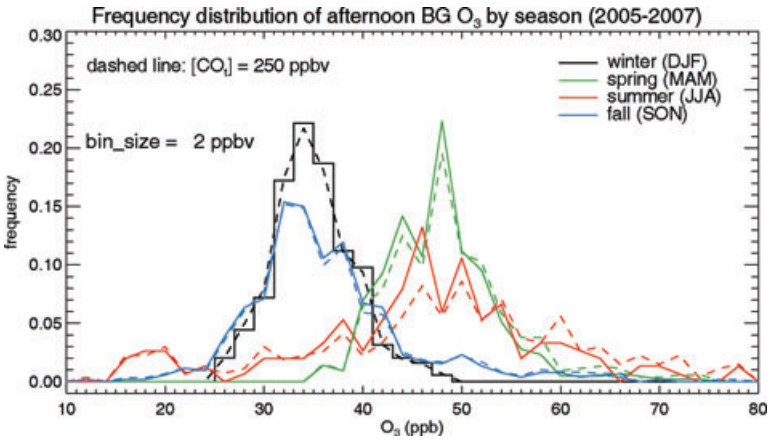

Fig. 9. Frequency distribution of afternoon O_3 for the background air masses identified at Miyun by seasons (2005–2007). The dashed line shows the distribution of background O_3 if $[CO_t]$ is set uniformly at 250 ppbv in each season.

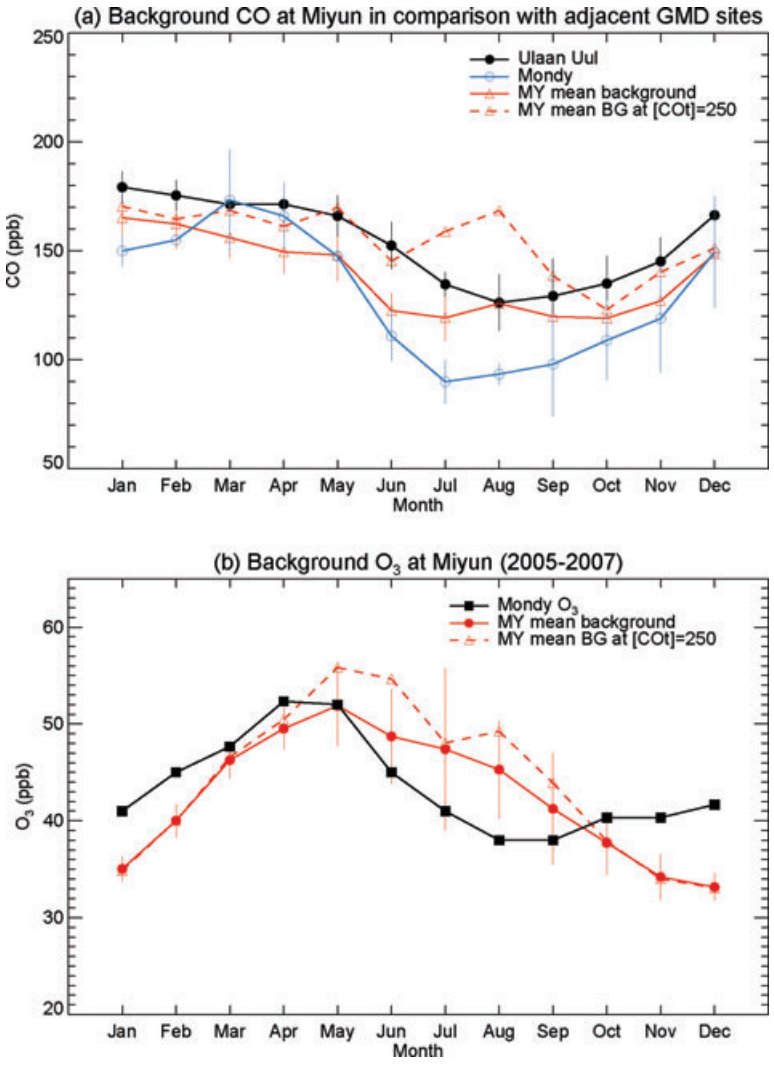

Fig. 10. Monthly mean background CO (a) and O_3 (b) identified at Miyun as compared with monthly mean observations at several adjacent continental background sites. The vertical lines indicate the uncertainties of the background for individual months.

and Mondy sites are located upwind of Miyun during periods of northwesterly prevailing winds. The seasonality of background CO at Miyun is similar to that at UUM. Background CO identified at Miyun ranges from 150 to 200 ppb, with minima in autumn and maxima in winter. This seasonality in background CO is consistent with the effects of OH reactivity on CO lifetime (Lee et al., 2006). The spring maximum in CO at Mondy is attributed to the influence of biomass burning over Siberia (Pochanart et al. 2003). Background CO at Miyun is generally lower by 5–10 ppb than mean CO at UUM, but 10–20 ppb higher than that at Mondy except in spring. The differences are largely within the standard deviation of monthly mean CO at UUM and Mondy and the uncertainty in Miyun background introduced by $[CO_t]$. When $[CO_t]$ is set of 250 ppbv, monthly mean background CO derived at Miyun increased by 10–20 ppb for non-summer months.

In contrast to the summer maximum of overall O_3 at Miyun, background O_3 identified at the site (Fig. 10b) shows pronounced maxima (47 ppb) in spring (MAM) with minima (35 ppb) in winter. This seasonal cycle is consistent with the seasonality of O_3 at many background continental sites in northern middle latitudes and with ozonesonde data (Logan, 1999; Monks, 2000). Similar to CO, background O_3 derived for summer is subject to large uncertainties and not discussed here. When $[CO_t]$ is set of 250 ppbv, monthly mean background O_3 derived at Miyun increased by 5–10 ppb in spring and fall. Background O_3 in winter is less sensitive to $[CO_t]$. The springtime maximum in background O_3 is attributed to stratosphere/troposphere exchange which peaks in spring in the northern hemisphere (Appenzeller et al., 1996) combined with a contribution from photochemical production (Liu et al., 1987). Background O_3 at Miyun is lower by 6–10 ppb compared to O_3 levels at Mondy, although the seasonal cycle at the two sites is similar. Mondy site is at higher elevation (2 km a.s.l.) than Miyun, which generally receive air from a higher altitude with higher background O_3 than at the surface. Pochanart et al. (2003) noticed that O_3 levels at

Mondy were significantly higher compared to most European background sites and attributed the differences to influences of marine air masses with low O_3 transported over long distances to the European background sites.

3.3. O_3–CO relationship in different pollution plumes

In this section, we examine the O_3–CO relationship for pollution plumes sampled at Miyun between June and September in each year, the typical time period with active photochemical production of ozone as indicated by the overall positive relationship between O_3 and CO (Fig. 5). Since pollution plumes sampled at Miyun are characterized typically by concurrent, sharp enhancement in mixing ratios of O_3 and CO in the afternoon, we adopted the following criteria to identify the plumes. For a measurement day to be chosen as a plume day, it is required that (1) the peak of CO during the course of the day had to occur in the afternoon and coincide with the peak of O_3 and (2) the peak of CO and O_3 had to exceed the respective median mixing ratio for the month. A total of 42 measurement days met both criteria, accounting for 15% of the total measurement days for the period of interest. The simultaneous peaks of O_3 and CO in each plume day are used to represent individual plumes. Figure 11 shows the CO–O_3 relationships for the 42 plumes. Mixing ratios of O_3 for all plumes identified range from 60 to 185 ppb, with CO between 500 and 2200 ppb.

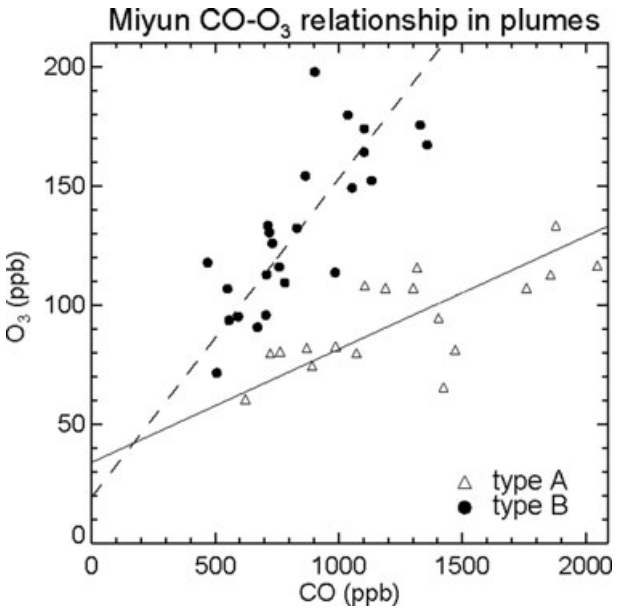

Fig. 11. Correlation between CO and O_3 in two types of pollution plumes observed at Miyun in summer. The type-A plumes are indicated by open triangles and the type-B plumes by filled circles. See Section 3.3 for descriptions of the two types of plumes.

Two distinct populations are evident in Fig. 11, representing presumably two types of plumes with different characteristics of emission and chemistry. For purposes of this discussion, the two populations are referred to as type-A and type-B plumes. As all the plumes are from the same photochemically active period in each year (June–September) when background mixing ratios of CO and O_3 are low (Fig. 10), we do not subtract off background in deriving the dO_3/dCO correlation slope. The O_3–CO correlation slope (dO_3/dCO) for type-A plumes is 0.047 ± 0.008 ppb ppb^{-1} ($n = 18$, $r = 0.72$), lower by a factor of 3 than the value of 0.133 ± 0.017 ppb ppb^{-1} for type-B plumes ($n = 24$, $r = 0.79$). Mean mixing ratios of O_3, CO and their correlation slopes in type-A and type-B plumes are summarized in Table 1. The table includes mean SO_2, NO_y and NO for the two types of plumes in 2007, the first year for which these measurements became available at Miyun. A variance test (t-test) was conducted to determine if mean pollutant levels between the two types of plumes are statistically significant. The p-values of the t-test are included in Table 1, with p less than or equal to 0.05 (one-tailed; 95% confidence interval) considered as statistically significant. As shown in Table 1, mean mixing ratios of O_3 and CO are 94 and 1261 ppb respectively for type-A plumes, and 132 and 840 ppb, respectively for type-B plumes. The differences in both CO and O_3 are statistically significant at 95% confidence interval. The NO/NO_y ratio, indicating the aging of air masses (Munger et al., 1996), is 0.02 in type-A plumes and 0.0016 in type-B plumes, and the difference is statistically significant ($p < 0.05$). This suggests that type-B plumes are more aged than type-A plumes, representing presumably pollution transported over longer distances from upwind urban areas. Indeed, type-B plumes have on average much higher levels of NO_y ($p < 0.05$), tracers dominated by transportation sources characteristic of urban and industrial environments. In contrast, the very high levels of CO in type-A plumes reflect possible emissions from sources involving inefficient combustion in the rural environment, such

Table 1. Mean chemical compositions (mixing ratios in ppb) and species correlation slopes (ppb ppb^{-1}) for two types of pollution plumes identified at Miyun in summer. The p-values of the variance test (t-test) of the differences in the two types of plumes are included

	O_3	CO	O_3–CO slope	SO_2	NO_y	NO	NO/NO_y ratio
Type-A plumes	93.7	1260.5	0.047	9.3	18.6	0.175	0.02
Type-B plumes	131.5	840.1	0.133	11.7	40.3	0.074	0.0016
p-Value (one tailed) for difference	0.0001	0.0002	1e-6	0.25	0.03	0.06	0.03

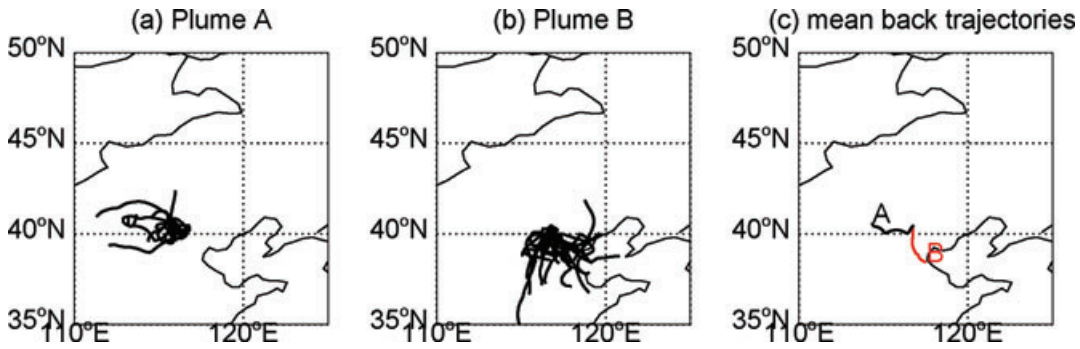

Fig. 12. Two-day back trajectories of the type-A plumes (a), type-B plumes (b). (c) The mean trajectories of the two types of plumes (type-A plumes in black and type-B plumes in red).

as open burning of biomass and domestic burning of biofuel. Although SO_2 is on average higher in type-A plumes, the difference is not statistically significant at 95% confidence interval, suggesting there may be relatively smaller gradient in SO_2 emissions from urban to rural areas given that coal fired power plants are largely surrounding Beijing and heavy-duty diesel vehicles, an important source of SO_2 in cities, are prohibited from entering Beijing urban area during the day. Photochemical production of O_3 and its build up is expected to be more effective in aged urban plumes than biomass burning plumes, consistent with higher levels of O_3 observed in type-B plumes.

The Hybrid Single-Particle Lagrangian Integrated Trajectory (HYSPLIT) model (version 4.9) (http://www.arl.noaa.gov/HYSPLIT.php) (Draxler and Hess, 1998) was employed in this study to calculate 48-h (2-day) backward trajectories of observations identified in the type-A and type-B plumes. The meteorological data employed to calculate the back trajectories are GDAS reanalysis data at $1^\circ \times 1^\circ$ spatial resolution. The back trajectories are calculated with the initial height of 6 m and time steps of 1 h. This corresponded to 18 back trajectories for type-A plumes (Fig. 12a) and 24 back trajectories for type-B plumes (Fig. 12b). Mean back trajectories of the two types of plumes are presented in Fig. 12c. Air masses in type-A plumes originated from west and southwest of the Miyun site and circulated around the local area of the site (Fig. 11a). Figure 8 indicates that biomass burning hot spots are located to the west and southwest of the site in summer, suggesting biomass burning influences on the type-A plumes. Air masses in type-B plumes originated from south and southeast of the site where urban areas such as Beijing and Tianjin are located. Given their different chemical compositions and trajectory analysis, we conclude that two types of pollution plumes with significantly different O_3–CO correlation slopes are distinguished at Miyun, one representing biomass burning pollution (i.e. type-A plumes, $O_3/CO = 0.047$ ppb ppb^{-1}) and the other reflecting aged urban pollution (i.e. type-B plumes, $O_3/CO = 0.133$ ppb ppb^{-1}). Biomass burning plumes (i.e. type-A plumes) identified here are likely associated with open field burning of crop residues.

The O_3–CO correlation slopes for the two types of plumes represent the lower and upper bounds for O_3–CO relationships observed at Miyun. When all the Miyun observations from June to September are considered, the correlation between O_3 and CO is weak and the mean O_3–CO slope is $\sim$0.07 ppb ppb^{-1}. The O_3–CO slope of 0.133 ppb ppb^{-1} for the aged urban pollution plumes is among the highest reported previously in the literature for O_3–CO ratios in China in summer (Wang et al., 2001; Gao et al, 2005; Meng et al., 2009). It is however much smaller than the O_3–CO ratio observed at many surface sites in Japan, North America and Europe, typically ranging from 0.2 to about 0.4 ppb ppb^{-1} (Chin et al., 1994; Parrish et al., 1998; Pochanart et al., 1999; Mauzerall et al., 2000; Mao and Talbot, 2004), as the CO levels in the aged urban plumes ($\sim$800 ppb) sampled at Miyun are much higher than those observed in western countries. Mauzerall et al. (2000) adopted the O_3–CO slope of 0.3 ppb ppb^{-1} to estimate the export of O_3 from Asia through direct scaling of the slope by CO emissions. From the large gradient in O_3–CO slopes sampled at Miyun for different types of air masses and the departure from the typical slope of 0.3 ppb ppb^{-1} reported elsewhere, we argue that such direct interpretation of the mean slope to deduce O_3 production rate is subject to large uncertainties.

4. Concluding remarks

The Miyun station, a rural site 100 km northeast of Beijing, provides continuous, high quality measurements for a suite of important gases (CO, CO_2, O_3, SO_2, NO and NO_y) over a relatively long period. In this paper we have presented seasonal variations of CO, O_3 and their relationships as observed at Miyun. Based on concentrations of CO and prevailing wind directions, we identified two distinct classes of air masses reaching the site. One reflects clean continental air masses from the north with low concentrations of CO (less than 200 ppb), the other, distinguished by high levels of CO (>800 ppb), represents polluted air from the south. The contrast indicates that at the Miyun site, we can sample both the clean background air and the polluted

regional air over north China. Because of the seasonal change in synoptic pattern, the relatively clean continental air masses were sampled more frequently in winter and the polluted air masses more often in summer.

Monthly mean mixing ratios of afternoon CO (1200–1800 local time) varied between 500 and 1000 ppb. The median and lower percentiles of CO, influenced by the relative frequency of relatively clean, northerly air masses, show summer maxima of 500–600 ppb with winter minima of 300–400 ppb. In contrast, the mean and higher percentiles (>67%) of CO, reflecting the relative frequency of influences of urban pollution plumes at the site, have two peaks, one in winter and the other in early summer (June–July), and minima during the transition seasons (April–May and August–September). Mixing ratios of O_3 at Miyun show a clear seasonal pattern with minima in winter and maxima in early summer (June). Monthly mean levels of afternoon O_3 were 85 ppb in June as compared to about 45 ppb in January. Significant interannual variability is found for CO in all months, while the interannual variability of O_3 is much smaller and not significant from late fall through early spring (November–March). The interannual variability of CO and O_3 can be attributed to the interannual variability of meteorology and emissions from biomass burning.

We expect that background air masses sampled at Miyun will have distinctly lower levels of CO than polluted regional/local air masses. The presence of a narrow and pronounced peak at the lower end of the frequency distribution of CO in winter, spring and fall suggests that background air masses are frequently sampled at Miyun in these seasons. The lack of such a peak in summer suggests that summertime measurements at this site may not be suitable for identifying the background since the site is located downwind of the Beijing urban area in summer under the prevailing southwesterly winds and is consequently poorly located to sample the relatively clean continental air masses frequently enough. Background air masses are found to account for 43, 33 and 35% of all afternoon observations in winter, spring and fall, respectively.

Background CO follows a lognormal distribution in non-summer seasons. The distribution is similar in winter and spring with a peak at 150 ppbv. The peak shifts to 90 ppbv in fall. This seasonality in background CO is consistent with the effects of OH reactivity on CO lifetime (Lee et al., 2006). The distribution of background O_3 is close to normal in non-summer seasons. It peaks between 30 and 40 ppbv in winter and fall and 45–50 ppbv in spring. The springtime maximum in background O_3 is attributed to stratosphere/troposphere exchange which peaks in spring in the northern hemisphere combined with a contribution from photochemical production. The seasonality and magnitude of background CO and O_3 derived at Miyun are consistent with observations at upwind remote continental sites.

O_3 and CO at Miyun have moderate to strong negative correlations in winter, moderate to strong positive correlations in summer and early fall (June–September, except in July). The correlations of O_3 and CO are weak and not statistically significant in spring, fall and July. The seasonal transition in the O_3–CO correlation is consistent with observations at other surface sites. The O_3–CO correlation slope at Miyun in summer is about 0.07 ppb ppb^{-1} on average, significantly lower than the typical slope of 0.3 ppb ppb^{-1} reported for developed countries. The O_3–CO correlation slope shows large gradients for different types of air masses. It is 0.133 and 0.047 ppb ppb^{-1} in aged urban pollution plumes and biomass burning plumes, respectively, representing the lower and upper bounds for O_3–CO relationships observed at Miyun in summer. The large variability in O_3–CO correlations observed at the site implies that the conventional method of direct scaling the mean O_3–CO slope by CO emissions to deduce O_3 production rate is subject to large uncertainties if applied for China.

5. Acknowledgments

This research was supported by the National Science Foundation, grant ATM-0635548 and funds from the Harvard University Smeltzer Fund and an anonymous private foundation. Y.X. Wang and J.M. Hao was supported by the National Science Foundation of China (Grant No. 20437010) and Program of Research on Key Technology of Environmental Pollution Control and Quality Improvement (2007DFC90170).

References

Appenzeller, C., Holton, J. R. and Rosenlof, K. H. 1996. Seasonal variation of mass transport across the tropopause. *J. Geophys. Res.* **101**, 15071–15078.

Chin, M., Jacob, D. J., Munger, J. W., Parrish, D.D. and Doddridge, B.G. 1994. Relationship of ozone and carbon monoxide over North America. *J. Geophys. Res.* **99**(D7), 14565–14573.

Cooper, O. R., Moody, J. L., Parrish, D. D., Trainer, M., Holloway, J. S. and co-authors. 2002. Trace gas composition of midlatitude cyclones over the western North Atlantic Ocean: a seasonal comparison of O_3 and CO. *J. Geophys. Res.* **107**(D7), doi:10.1029/2001JD000902.

Ding, A. J., Wang, T., Thouret, V., Cammas, J.-P. and Nédélec, P. 2008. Tropospheric ozone climatology over Beijing: analysis of aircraft data from the MOZAIC program. *Atmos. Chem. Phys.* **8**, 1–13.

Draxler, R. R. and Hess, G.D. 1998. An overview of the HYSPLIT 4 modelling system for trajectories, dispersion, and deposition. *Aust. Meterol. Mag.* **47**, 295–308.

Fu, T.-M., Jacob, D. J., Palmer, P. I., Chance, K., Wang, Y. X. and co-authors. 2007. Space-based formaldehyde measurements as constraints on volatile organic compound emissions in East and South Asia. *J. Geophys. Res.* **112**, D06312, doi:10.1029/2006JD007853.

Gao, J., Wang, T., Ding, A. and Liu, C. 2005. Observations study of ozone and carbon monoxide at the summit of mount Tai (1534m a.s.l.) in central-eastern China. *Atmos. Environ.* **39**, 4779–4791.

GLOBALVIEW-CO. 2009. Cooperative Atmospheric Data Integration Project – Carbon Monoxide. CD-ROM, NOAA ESRL, Boulder, Colorado [Also available on Internet via anonymous FTP to ftp.cmdl.noaa.gov, Path: ccg/co/GLOBALVIEW]

Hirsch, R. M. and Gilroy, E. J. 1984. Methods of fitting a straight line to data: examples in water resources. *Water Resour. Bull.* **20**, 705–711.

Jaffe, D. and Ray, J. 2007. Increase in surface ozone at rural sites in the western US. *Atmos. Environ*. **41**(26), 5452–5463.

Kleinman, L., Lee, Y. N., Springston, S. R., Nunnermacker, L., Zhou, X. and coauthors. 1994. Ozone formation at a rural site in the southeastern United States. *J. Geophys. Res.* **99**(D2), 3469–3482.

Lee, B. H., Munger, J. W., Wofsy, S. C. and Goldstein, A. H. 2006. Anthropogenic emissions of nonmethane hydrocarbons in the northeastern United States: measured seasonal variations from 1992–1996 and 1999–2001. *J. Geophys. Res.* **111**, D20307, doi:10.1029/2005JD006172.

Liang, J., Horowitz, L., Jacob, D., Wang, Y., Fiore, A. and co-authors. 1998. Seasonal budgets of reactive nitrogen species and ozone over the United States, and export fluxes to the global atmosphere. *J. Geophys. Res.* **103**(D11), 13435–13450.

Lin, C. Y., Jacob, D. J., Munger, J. W. and Fiore A. M. 2000. Increasing background ozone in surface air over the United States. *Geophys. Res. Lett.* **27**, 3465–3468.

Lin, W., Xu, X., Zhang, X. and Tang, J. 2008. Contribution of pollutants from North China Plain to surface ozone at the Shangdianzi GAW station. *Atmos. Chem. Phys.* **8**, 5889–5898.

Liu, S. C., Trainer, M., Fehsenfeld, F. C., Parrish, D. D., Williams, E. J. and co-authors. 1987. Ozone production in the rural troposphere and the implications for regional and global ozone distributions. *J. Geophys. Res.* **92**, 4191–4207.

Logan, J. A. 1989. Ozone in rural areas of the United States. *J. Geophys. Res.* **94**, 8511–8532.

Logan, J. A. 1999. An analysis of ozonesonde data for the troposphere: recommendations for testing 3-D models and development of a gridded climatology for tropospheric ozone. *J. Geophys. Res.* **104**, 16115–16150.

Luo, C., St. John, J. C., Zhou, X., Lam, K. S., Wang, T. and co-authors. 2000. A nonurban ozone air pollution episode over eastern China: observations and model simulations. *J. Geophys. Res.* **105**(D2), 1889–1908.

Mao, H. and Talbot, R. 2004. O_3 and CO in New England: temporal variations and relationships. *J. Geophys. Res.* **109**(D2), 1304, doi:10.1029/2004JD004913.

Mauzerall, D. L., Narita, D., Akimoto H., Horowitz L., Walters S. and co-authors. 2000. Seasonal characteristics of tropospheric ozone production and mixing ratios over East Asia: a global three-dimensional chemical transport model analysis. *J. Geophys. Res.* **105**, 17895–17910.

Meng, Z. Y., Xu, X. B., Yan, P., Ding, G. A., Tang, J., and co-authors. 2009. Characteristics of trace gaseous pollutants at a regional background station in Northern China. *Atmos. Chem. Phys.* **9**, 927–936.

Monks, P. S. 2000. A review of the observations and origins of the spring ozone maximum. *Atmos. Environ.* **34**, 3545–3561.

Munger, J., Wofsy, S., Bakwin, P., Fan, S.-M., Goulden, M. and co-authors. 1996. Atmospheric deposition of reactive nitrogen oxides and ozone in a temperate deciduous forest and a subarctic woodland 1. Measurements and mechanisms. *J. Geophys. Res.* **101**(D7), 12639–12657.

Ohara, T., Akimoto, H., Kurokawa, J., Horii, N., Yamaji, K. and co-authors. 2007. An Asian emission inventory of anthropogenic emission sources for the period 1980–2020. *Atmos. Chem. Phys.* **7**, 4419–4444.

Oltmans, S. J., Lefohn, A. S., Scheel, H. E., Harris, J. M., Levy II, H. and co-authors. 1998. Trends of ozone in the troposphere. *Geophys. Res. Lett.* **25**, 139–142.

Parrish, D. D., Trainer, M., Buhr, M. P., Watkins, B. A. and Fehsenfeld, F. C. 1993. Export of North American ozone pollution to the North Atlantic Ocean. *Science* **259**, 1436–1439.

Parrish, D. D., Trainer, M., Holloway, J. S., Yee, L. E., Warshawsky, M. S. and co-authors. 1998. Relationships between ozone and carbon monoxide at surface sites in the North Atlantic region. *J. Geophys. Res.* **103**, 13357–13376.

Pfister, G. G., Emmons, L. K., Hess, P. G., Honrath, R., Lamarque, J. F. and co-authors. 2006. Ozone production from the 2004 North American boreal fires. *J. Geophys. Res.* **111**, D24S07, doi:10.1029/2006JD007695.

Pochanart, P., Hirokawa, J., Kajii, Y., Akimoto, H. and Nakao, M. 1999. Influence of regional-scale anthropogenic activity in Northeast Asia on seasonal variations of surface ozone and carbon monoxide observed at Oki, Japan. *J. Geophys. Res.* **104**, 3621–3631.

Pochanart, P., Akimoto, H., Kajii, Y., Potemkin, V. M. and Khodzher, T. V. 2003. Regional background ozone and carbon monoxide variations in remote Siberia/east Asia. *J. Geophys. Res.* **108**(D1), 4028, doi:10.1029/2001JD001412.

Poulida, O., Dickerson, R. R., Doddridge, B. G., Holland, J. Z., Wardell, R. G. and co-authors. 1991. Trace gas concentrations and meteorology in rural Virginia, 1. ozone and carbon monoxide. *J. Geophys. Res.* **96**(D12), 22461–22475.

Real, E., Law, K. S., Schlager, H., Roiger, A., Huntrieser, H. and co-authors. 2008. Lagrangian analysis of low altitude anthropogenic plume processing across the North Atlantic. *Atmos. Chem. Phys.* **8**, 7737–7754.

Streets, D. G., Zhang, Q., Wang, L., He, K., Hao, J. and co-authors. 2006. Revisiting China's CO emissions after TRACE-P: synthesis of inventories, atmospheric modeling, and observations. *J. Geophys. Res.* **111**, D14306, doi:10.1029/2006JD007118.

Van Der Werf, G. R., Randerson, J. T., Giglio, L., Collatz, G. J., Kasibhatla, P/ S. and co-authors. 2006. Interannual variability in global biomass burning emissions from 1997 and 2004. *Atmos. Chem. Phys.* **6**, 3423–3441.

Wang, T., Cheung, V. T. F., Anson, M. and Li, Y.S. 2001. Ozone and related gaseous pollutants in the boundary layer of eastern China: overview of the recent measurements at a rural site. *Geophys. Res. Lett.* **28**, 2373–2376.

Wang, T., Cheung, T. F., Li, Y. S., Xu, X. M. and Blake, D. R. 2002. Emission characteristics of CO, NO_x, SO_2 and indications of biomass burning observed at a rural site in eastern China. *J. Geophys. Res.* **107**, doi:10.1029/2001JD000724.

Wang, T., Ding, A. J., Blake, D. R., Zahorowski, W., Poon, C. N. and co-authors. 2003. Chemical characterization of the boundary layer outflow of air pollution to Hong Kong during February–April 2001. *J. Geophys. Res.* **108**(D20), 8787, doi:10.1029/2002JD003272.

Wang, T., Wong, C. H., Cheung, T. F., Blake, D. R., Arimoto, R. and co-authors. 2004. Relationships of trace gases and aerosols and the emission characteristics at Lin'an, a rural site in

eastern China during spring 2001. *J. Geophys. Res.* **109**, D19S05, doi:10.1029/2003JD004119.

Wang, T., Guo, H., Blake, D. R., Kwok, Y. H., Simpson, I. J. and co-authors. 2005. Measurements of trace gases in the inflow of South China Sea background air and outflow of regional pollution at Tai O, Southern China. *J. Atmos. Chem.* **52**, 295–317, doi:10.1007/s10874–005-2219-x.

Wang, T., Wong, A., Tang, J., Ding, A., Wu, W. S. and co-authors. 2006b. On the origin of surface ozone and reactive nitrogen observed at a remote mountain site in the northeastern Qinghai-Tibetan Plateau, western China. *J. Geophys. Res.* **111**, doi:10.1029/2005JD006527.

Wang, Y. X., McElroy, M. B., Martin, R. V., Streets, D. G., Zhang, Q. and co-authors. 2007. Seasonal variability of NO_x emissions over east China constrained by satellite observations: implications for combustion and microbial sources. *J. Geophys. Res.* **112**, D06301, doi:10.1029/2006JD007538.

Wang, Y. X., McElroy, M. B., Munger, J. W., Hao, J., Ma, H. and co-authors. 2008. Variations of O_3 and CO in summertime at a rural site near Beijing. *Atmos. Chem. Phys.* **8**, 6355–6363.

Zhang, Q., Streets, D. G., He, K., Wang, Y. X., Richter, A. and co-authors. 2007. NO_x emission trends for China 1995–2004: the view from the ground and the view from space. *J. Geophys. Res.* **112**, D22306, doi:10.1029/2007JD008684.

Zhang, L., Jacob, D. J., Boersma, K. F., Jaffe, D. A., Olson, J. R. and co-authors. 2008. Transpacific transport of ozone pollution and the effect of recent Asian emission increases on air quality in North America: an integrated analysis using satellite, aircraft, ozonesonde, and surface observations. *Atmos. Chem. Phys.* **8**, 6117–6136.